STEM CELLS AND DEVELOPMENT
Volume 21, Number 15, 2012

DOI: 10.1089/scd.2011.0437

Netrin-1-Mediated Axon Guidance in Mouse Embryonic Stem Cells Overexpressing Neurogenin-1

Gerhard W. Hill, III,[1,*] Erin K. Purcell,[1] Liqian Liu,[1] John Matthew Velkey,[2,†] Richard A. Altschuler,[1,2] and Robert Keith Duncan[1]

Stem cell therapy holds great promise for treating neurodegenerative disease, but major barriers to effective therapeutic strategies remain. A complete understanding of the derived phenotype is required for predicting cell response once introduced into the host tissue. We sought to identify major axonal guidance cues present in neurons derived from the transient overexpression of neurogenin-1 (*Neurog1*) in mouse embryonic stem cells (ESCs). *Neurog1* upregulated the netrin-1 axon guidance receptors DCC (deleted in colorectal cancer) and neogenin (NEO1). Quantitative polymerase chain reaction results showed a 2-fold increase in NEO1 mRNA and a 36-fold increase in DCC mRNA in *Neurog1*-induced compared with control ESCs. Immunohistochemistry indicated that DCC was primarily expressed on cells positive for the neuronal marker TUJ1. DCC was preferentially localized to the cell soma and growth-cones of induced neurons. In contrast, NEO1 expression showed less specificity, labeling both TUJ1-positive and TUJ1-negative cells as well as uninduced control cells. Axonal outgrowth was directed preferentially toward aggregates of HEK293 cells secreting a recombinant active fragment of netrin-1. These data indicate that DCC and NEO1 are downstream products of *Neurog1* and may guide the integration of *Neurog1*-induced ESCs with target cells secreting netrin-1. Differential expression profiles for netrin receptors could indicate different roles for this guidance cue on neuronal and non-neuronal cells.

Introduction

Neurodegeneration and nerve injury lead to a debilitating loss of sensory, motor, and cognitive function. Current therapies seek to restrain the progression of disease or augment residual function, but neither of these approaches addresses the root problem of neuronal loss. In light of the limited capacity of the nervous system to repair itself, there is a vital need for effective regenerative treatments. One potential therapeutic avenue is replacement of injured neurons with those derived from embryonic stem cells (ESCs) [1]. A stem cell-based approach faces many challenges before its practical, widespread implementation as a therapeutic tool. Progress toward clinical application will require differentiation of tissue-specific phenotypes that recapitulate the full neurophysiological features of the cells being replaced. These features include the key morphological, electrical, and neurochemical properties that govern neuron function as well as the axon growth and guidance cues that undoubtedly will be necessary to optimize integration with host tissue.

Several methods have been established to direct the differentiation of ESCs toward neural cell fates [2], but genetic induction holds the promise of guiding ESCs toward a specific neural lineage [3]. Recently, a reliable method of rapidly inducing a neuronal fate from mouse ESCs was described [4]. Overexpression of the proneural gene neurogenin-1 (*Neurog1*) in mouse ESCs resulted in the rapid adoption of a functional glutamatergic phenotype [5,6]. The electrical and neurochemical properties of the induced neurons were similar to those of endogenous cranial sensory neurons naturally derived from the *Neurog1*-lineage. The next challenge is to identify the intrinsic cues that control the outgrowth and integration of the stem cell-derived neurons.

Neurite extension, branching, and pathfinding are controlled by a combination of diffusible signals and contact cues [7,8]. Netrins are a family of conserved secreted proteins that influence the neurite length, axon guidance, cell migration, and tissue morphology [9]. These proteins act as bifunctional guidance molecules, attracting or repelling axons depending on receptor configuration in the target neuron. Attraction is mediated by the receptor DCC (deleted in colon

[1]Department of Otolaryngology, Kresge Hearing Research Institute, University of Michigan, Ann Arbor, Michigan.
[2]Department of Cell and Developmental Biology, University of Michigan, Ann Arbor, Michigan.
*Current affiliation: Division of Otolaryngology, Department of Surgery, Texas A&M Health Science Center College of Medicine, Scott & White Memorial Hospital, Temple, Texas.
†Current affiliation: Department of Cell Biology, Duke University, Durham, North Carolina.

cancer), whereas repulsion involves the UNC5 receptor family [10,11]. Another netrin receptor, neogenin (NEO1), bears structural homology to DCC and also participates in bifunctional guidance [12], but NEO1 appears to regulate additional cellular processes, including neural tube formation, myogenesis, angiogenesis and organogenesis of the lung, gut, and kidney [13].

Several observations support a role for netrin-1 in guiding projections from *Neurog1*-induced ESCs. First, a genome-wide bioinformatics analysis identified DCC as a possible transcriptional target of Neurog1 [14]. Second, mouse mutants with combined deletions of *Neurog1* and *Neurog2* exhibit reduced DCC expression and axonal pathfinding defects that may be related to aberrant netrin signaling [15]. Third, netrin-1 plays an important role in the development of spiral ganglion neurons (SGNs) [16,17] and dorsal root ganglion neurons [18], 2 classes of sensory neurons that rely on *Neurog1* expression for fate specification [19,20]. Based on these observations, we hypothesized that netrin-1 is a key guidance molecule regulating axonal outgrowth of *Neurog1*-induced ESCs. Results from the current study indicate that netrin-1 serves as an attractive guidance cue for *Neurog1*-induced cells and that this effect is likely mediated by DCC expressed in the growth cones of derived neurons.

Materials and Methods

Stem cell culture and neuronal induction

A reverse tet-transactivator system was used to force the expression of *Neurog1* in a mouse ESC line (N7), as previously described [5]. N7 cells were maintained and expanded in the growth medium consisting of the DMEM (Invitrogen), 10% heat-inactivated fetal bovine serum (Atlanta Biologicals), 5% ESC supplement (DMEM with 24% HEPES buffer, 4 mg/mL L-glutamine, and 70 ng/mL beta-mercaptoethanol), and 0.5 μg/mL the leukemia inhibitory factor (Millipore). Selection antibiotics puromycin (1.5 μg/mL) and G418 (350 μg/mL) were added to maintain a clonal culture of stably transfected cells. For differentiation, cells were dissociated and seeded in a serum-free differentiation medium (80:20 medium), which included 80% F12/DMEM 1:1 (Invitrogen), 20% Neurobasal (Invitrogen), 10 mM sodium pyruvate (Invitrogen), 0.8% N2 supplement (Invitrogen), and 0.4% B27 supplement (Invitrogen). Culture wells and Thermanox coverslips were coated with 0.1% gelatin (Sigma) before seeding. *Neurog1* expression was induced with 1 μg/mL doxycycline in the 80:20 medium for 3 days with half-volume medium exchanges each day. Uninduced control cells were cultured in parallel in the 80:20 medium without doxycycline. After 3 days, induced and uninduced cells were maintained an additional 2 days in the long-term medium consisting of the DMEM with 5% knockout serum replacement (Invitrogen) and 5% ESC supplement.

Gene expression assays

ESCs were seeded into 6-well tissue culture plates at a concentration of 5×10^5 cells per well. Total RNA was extracted from 5-day cultures of induced and uninduced cells under RNase free conditions using RNeasy Mini Kit (Qiagen) according to the manufacturer's instructions. RNA integrity and concentrations were obtained using the Agilent Bioanalyzer 2100. Samples were included in the study if the RNA integrity number, obtained from the 28S to 18S rRNA ratio, was 9.0 or higher. Total RNA from each treatment group was converted to cDNA using oligo(dT) primers and SuperScript III Reverse Transcriptase (Invitrogen) according to manufacturer's instructions. Quantitative polymerase chain reaction (qPCR) experiments were conducted using TaqMan Gene Expression Assays (Applied Biosystems). Thermocycling and data analysis were performed using an ABI PRISM 7900HT thermocycler and StepOnePlus analysis software (Applied Biosystems). Cycle threshold (CT) was determined for the genes of interest *Dcc* (Probe Assay Mm01262265_m1) and *Neo1* (Probe Assay Mm01176094_m1) and the housekeeping gene glyceraldehyde 3-phosphate dehydrogenase (*Gapdh;* Probe Assay Mm99999915_g1). Efficiency curves were generated from serially diluted concentrated cDNA obtained from induced ESC samples. Amplification efficiencies were 89% for *Gapdh,* 90% for *Dcc,* and 92% for *Neo1*. Changes in gene expression in induced cells were measured relative to uninduced cells using the ΔΔCT method [21]. Reactions were performed in triplicate. The standard deviation of triplicate CTs for all probes in all samples fell below 0.2. Results from 5 independent samples in each condition were averaged.

HEK293 cell culture and conditioned media

A chimeric fusion protein consisting of netrin structural domains V and VI conjugated to the human IgG1-Fc fragment was stably transfected into HEK293 cells (a generous gift from Dr. Elke Stein, Yale University). This recombinant netrin$^{VI\text{-}V\text{-}Fc}$ reproduces native netrin-1 behavior in axon guidance assays [22]. HEK cells were maintained in the DMEM, 10% fetal bovine serum (Invitrogen), and 1% penicillin-streptomycin (Invitrogen) with the selection antibiotics 200 μg/mL gentamicin (Hospira) and 12.5 μg/mL G418 (Sigma). Control blank HEK293 cell lines were maintained in the HEK medium without the selection antibiotics. In some cases, induced and uninduced ESCs were treated with the conditioned medium containing secreted recombinant netrin. The netrin-conditioned medium (NCM) was pooled from 3-day cultures of netrin-transfected HEK293 cells, whereas the control-conditioned medium (CCM) was obtained from untransfected HEK293 cells. The collected medium was centrifuged briefly to remove cellular debris, concentrated to ~10× using Amicon Ultra Centrifugal filters (10-kDa cutoff; Millipore), and stored at −80°C until use.

Immunohistochemistry

Induced and uninduced cells at 5 days in vitro were fixed with 4% paraformaldehyde and blocked with 0.1% Triton X-100 and 5% normal goat serum diluted in phosphate-buffered saline (PBS+). Cells were labeled with a rabbit or mouse antibody to the neuron-specific beta-III tubulin TUJ1 (Covance, MMS-435P or MRB-435P; 1:300–1:1,000) and goat polyclonal antibodies to DCC (R&D Systems; 0.5 μg/mL) and NEO1 (R&D Systems; 1 μg/mL). Primary antibodies were diluted in PBS+ and placed on the cells overnight at 4°C. To examine the binding of recombinant netrin, some preparations were treated with NCM or CCM for 90 min before fixation. AlexaFluor secondary antibodies (Invitrogen) were diluted in PBS+ (1:500) and applied for 1–2 h at room temperature. Cells were counterstained with Hoechst 33242 (Invitrogen) and mounted in Prolong Gold (Invitrogen).

Epifluorescence images were obtained using a Leica DM LB microscope outfitted with a cooled-CCD camera (MicroPublisher; Q Imaging). Confocal images were obtained using an Olympus Fluoview FV500. Postprocessing of original images was limited to cropping, rescaling, and merging separate color channels. ImageJ analysis software was used to create overlays of digital images, measure the neurite length, and quantify fluorescence intensity. Line scans were used to measure fluorescence intensity of antibody label along major neurites using methods similar to those described elsewhere [23,24]. To be considered for fluorescence quantification, neurites had to be (1) TUJ1-positive, (2) at least twice as long as the width of the soma, (3) devoid of obvious breaks, and (4) isolated from other TUJ1-positive cells. If >1 neurite was present, only the major (longest) neurite was analyzed. The intensity of the fluorescence signal along this major neurite was normalized to the maximum signal and averaged along consecutive segments, each measuring 10% of the total neurite length. In this way, the mean fluorescence along the neurite could be averaged among a population of neurons with different neurite lengths. Images were collected under constant exposure conditions and histograms were checked to prevent selecting images with saturated pixels. All specimens were prepared and analyzed in a single experimental session.

Turning assay with netrin-secreting HEK293 cells

Aggregates of HEK293 cells were produced from hanging drop cultures, as described elsewhere [25]. HEK cells were grown to confluence, dissociated with 0.25% trypsin with ethylenediaminetetraacetic acid (EDTA; Invitrogen), and triturated into a single-cell suspension at a concentration of 5×10^5 cells per mL. Small volume droplets (20 μL) of the cell suspension were placed on the undersurface of a tissue culture lid and incubated at 37°C with 5% CO_2 for 36–48 h until aggregates of cells were made in the drops hanging from the lid. The influence of netrin$^{VI\text{-}V\text{-}Fc}$ on axon outgrowth was examined by co-culturing *Neurog1*-induced ESCs with netrin-expressing HEK aggregates. Stem cells were first seeded in 6-well plates at a density of 7×10^4 cells and grown in the differentiation medium for 3 days. The differentiation medium was removed and netrin$^{VI\text{-}V\text{-}Fc}$-secreting or control HEK aggregates were transferred to the center of the well. Aggregates were held in place with a drop of rat-tail collagen type 1 (BD Biosciences) diluted to 25% with the HEK medium and allowed to gel. The long-term medium was added and the cells were co-cultured for up to 2 days.

Time-lapse images of induced ESCs co-cultured with netrin-HEK aggregates were captured using a Deltavision-RT Live Cell Imaging System configured for differential interference contrast enhancement. Images were acquired in 5 min intervals from multiple locations over a 4-h period immediately after introducing the netrin-secreting HEK aggregate. Separate preparations of induced ESCs were cultured with netrin-secreting or control HEK aggregates for 2 days, then fixed in 4% paraformaldehyde, and stained with anti-TUJ1. Overlapping images of TUJ1 immunoreactivity were collected covering a circular area (4-mm radius) surrounding the aggregate. The experimental condition of the combined image was blinded from the experimenter. The turning angle made between the initial segment of the neurite and a line drawn between the cell soma and the growth cone was measured in isolated TUJ1-positive neurites. The distance between the aggregate center and the cell soma was measured to determine if the distance from the netrin source impacted axon guidance. For inclusion in the study, neurites had to satisfy the criteria outlined for immunohistochemistry experiments and lay within 4 mm of the aggregate center without passing into or through the aggregate itself. The turning angle was collected from at least 3 separate preparations for each experimental condition.

Western blot analysis

Induced and uninduced cells were cultured for 5 days in vitro, washed with 1× HBSS, and incubated in the conditioned medium for 90 min. Cells were washed briefly with 1× HBSS and harvested in the lysis buffer (50 mM Tris-HCl, pH 8.0, with 120 mM sodium chloride, 5 mM EDTA, and 50 mM sodium floride) with 1× protease inhibitor cocktail (Sigma) and 250 μM okadaic acid added fresh upon use. Supernatants were collected by centrifugation and stored at −80°C until required. Protein concentration was determined by the Bradford Protein Assay using a DC Protein Assay Kit (BioRad). Proteins were separated by SDS-PAGE by loading 50 μg of total protein lysate onto a 4%–15% gradient gel. Separated proteins were electrophoretically transferred onto nitrocellulose membrane and blocked with 5% nonfat milk in 1× TTBS (0.1% Tween-20 in 1× TBS) for 1 h at room temperature. Membranes were then incubated with HRP-conjugated anti-human secondary antibody (Pierce; 1:10,000) to identify the Fc tag on netrin$^{VI\text{-}V\text{-}Fc}$ bound to cell lysates. Immunoreactive bands were stained using SuperSignal West Femto Maximum Sensitivity Substrate and a chemiluminescence signal detected using a Fluorochem SP imager (AlphaInnotech). Blots were stripped (Blot Fresh Western Blot Stripping Reagent; SignaGen) and reprobed with the primary antibody to GAPDH (Millipore; 1:3,000) as a loading control.

Results

Induction of Neurog1 *upregulates DCC and NEO1*

In an initial genome-wide expression screen, the netrin receptors *Dcc* and *Neo1* were upregulated by *Neurog1*, whereas *Unc5c* and *Dscam* were undetectable in uninduced cells and those overexpressing *Neurog1* for up to 48 h (data not shown). Based on these observations, we focused our attention on *Dcc* and *Neo1* for further analysis. qPCR was used to confirm *Neurog1* dependent changes in gene expression. Induced and uninduced cells were cultured for 3 days with and without doxycycline, respectively, and maintained for an additional 2 days in culture before analysis. PCR results from 5 replicate samples showed a 2.2-fold increase in *Neo1* and a 36.1-fold increase in *Dcc* after *Neurog1*-induced differentiation (Fig. 1). The change in expression for both receptors was significant compared to uninduced ESCs cultured in parallel (unpaired *t*-tests; *Dcc* $P<0.01$, *Neo1* $P<0.05$).

Real-time PCR response curves indicated that *Dcc* and *Neo1* were readily detectable in both induced and uninduced cells. Since both treatment groups were exposed to the differentiation medium with proneural supplements, it was

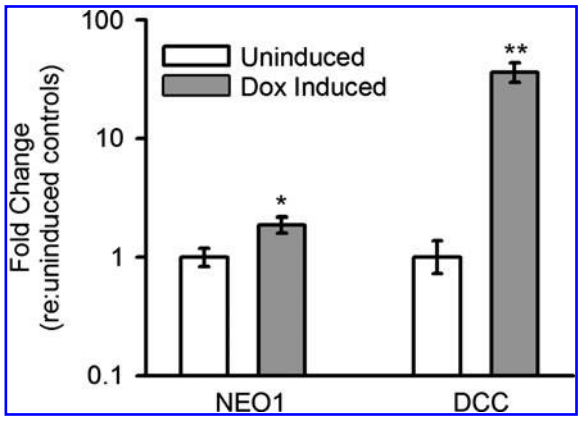

FIG. 1. Quantitative polymerase chain reaction (PCR) confirms the upregulation of netrin receptors following neurogenin-1 induction with doxycycline (Dox). *Neurog1*-induction resulted in a 2-fold increase in neogenin (NEO1) and a 36-fold increase in DCC (deleted in colorectal cancer) compared to uninduced control ESCs. $*P<0.05$, $**P<0.01$.

important to rule out any contribution from spontaneously differentiating ESCs. Previous reports have shown that the vast majority (>95%) of the uninduced ESCs are negative for the neuronal marker TUJ1, but positive for the pluripotency marker Oct3/4 [5,6], indicating a low rate of spontaneous differentiation after 2–3 days in culture and minimal leaky expression of *Neurog1* in the absence of doxycycline. However, after 12 days in this medium, ~10% of the ESCs spontaneously adopt a neuronal phenotype [6]. In our preparations, 5 days after plating, spontaneous differentiation into TUJ1-positive cells was extremely rare with an incidence of <0.001% and none of these extended long, thin neurites (Supplementary Fig. S1; Supplementary Data are available online at www.liebertpub.com/scd). Similar cultures exposed to doxycycline produced a large number of TUJ1-positive neurons. In a sampling of over 30 images from 9 preparations, ~10% of the cells were TUJ1-positive and extended one or more processes. This percentage of neural induction is somewhat smaller than previously reported for a modified *Neurog1*-ESC line stably expressing enhanced green fluorescent protein [5]. Nevertheless, differentiation efficiency was high enough to characterize derived neurons and to associate this with *Neurog1*-induction.

Samples were prepared for immunocytochemistry to identify and localize receptor expression at the protein level. Anti-NEO1 labeled both TUJ1-positive and negative cells in doxycycline-treated cultures (Fig. 2A–C) as well as undifferentiated control cells (Fig. 2D–F). NEO1 stained throughout the soma and neurite(s) of every TUJ1-positive neuron. In addition, NEO1 labeled many, though not all, TUJ1-negative cells. Labeling of these non-neuronal cell types was often punctate, appearing along the borders between adjacent cells. In contrast to NEO1, DCC was specifically expressed in TUJ1-positive cells (Fig. 3A–C) and was undetected in uninduced controls (Fig. 3D–F). There was a one-to-one correspondence between DCC- and TUJ1-labeled neurons.

Differential expression of DCC and NEO1 along TUJ1-positive neurites

The distribution of DCC and NEO1 labeling in TUJ1-positive neurons was different. While NEO1 had a uniform distribution along the neurons, DCC was preferentially expressed in the cell soma and the growth cone. These observations were quantified by averaging the relative intensity of staining along the neurons in consecutive segments each representing 10% of the total neurite length, where the junction of the cell soma and axon initiation was designated the 0% position and the growth cone 100%. Care was taken to avoid saturation of the CCD camera and to collect data under constant exposure conditions. The intensity of NEO1 was differentially distributed along the neurite [1-way analysis of variance (ANOVA), $P<0.001$], with intensity highest at the cell soma (Fig. 4A, B). A Dunnett's *post-hoc* analysis, using the terminal 10% of the neurite (the growth cone area) as the selected reference point, showed no significant difference in the staining level between the growth cone and the majority of the proximal axonal segments (10%–90%) (*P* values ranged from 0.15 to 1.00). However, the

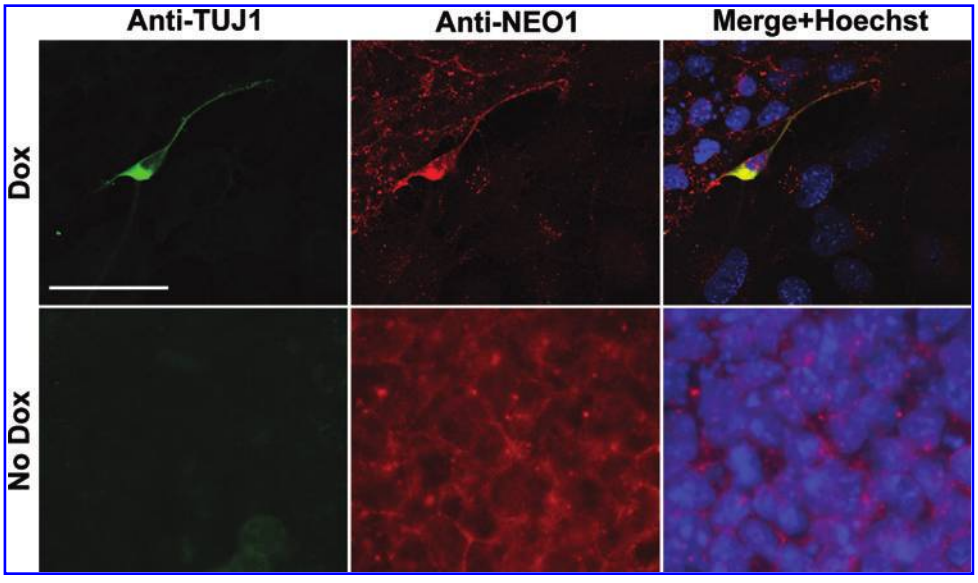

FIG. 2. Anti-NEO1 labeling of induced (doxycycline [Dox]) and uninduced (No Dox) mouse ESCs. Cultures were stained for TUJ1 (*green*) and NEO1 (*red*) and counterstained with Hoechst 33242 (*blue*). Anti-NEO1 stained neuronal and non-neuronal cells, including widespread labeling of uninduced ESCs. Images in Fig. 2 and elsewhere, while representative of responses through this and additional cultures, were taken from regions sparsely populated by neurons to show labeling detail along neurites and to reveal the extent of labeling in TUJ1+/− cells. Scale bar=50 μm. Color images available online at www.liebertpub.com/scd

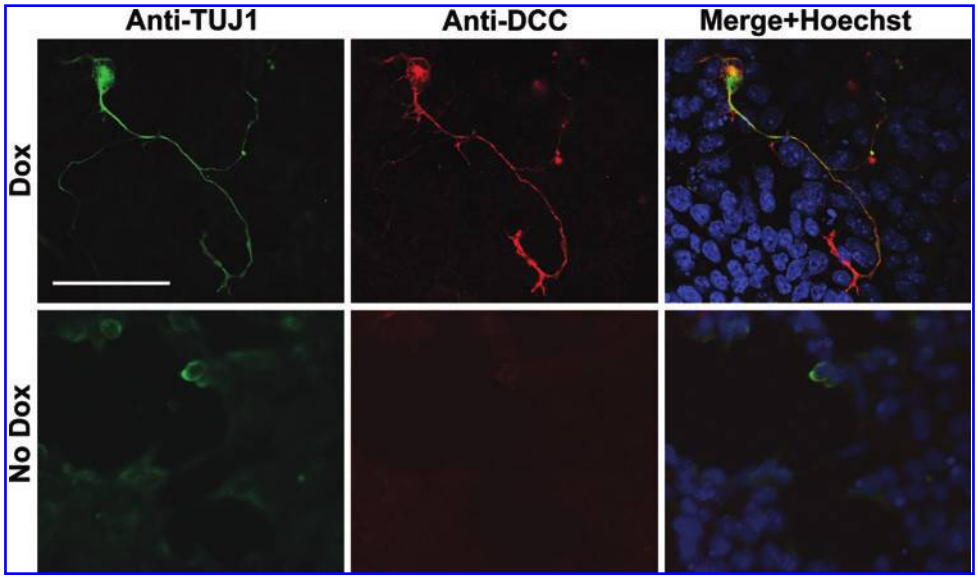

FIG. 3. Anti-DCC labeling of induced (Dox) and uninduced (No Dox) mouse ESCs. Cultures were stained for TUJ1 (*green*) and DCC (*red*) and counterstained with Hoechst 33242 (*blue*). Anti-DCC label was restricted to TUJ1-positive cells extending long, thin processes. Scale bar = 50 μm. Color images available online at www.liebertpub.com/scd

initial segment (0%–10%) was significantly brighter than the growth cone ($P < 0.01$). DCC staining was also differentially distributed along the neurite (1-way ANOVA, $P < 0.001$) (Fig. 5A, B), but in contrast to NEO1, DCC label was significantly more intense in the most distal and proximal segments compared to the intervening region of the axon (10%–80%) (Dunnett's *post-hoc* analysis, $P < 0.01$).

Netrin-1 attracts growth cones of stem cell derived-neurons

To examine the capacity for DCC and NEO1 receptors to bind netrin-1, we incubated induced and uninduced cells

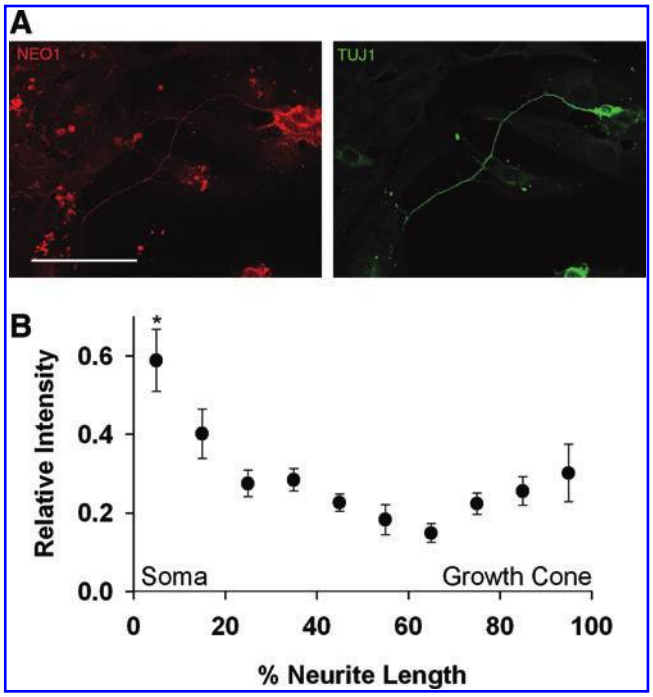

FIG. 4. NEO1 is preferentially localized to the cell soma in TUJ1-positive cells. **(A)** Induced cells were stained with anti-TUJ1 and anti-NEO1 as in Fig. 2. Labeling was brightest at the cell soma and uniformly distributed at a lower level along the neurite. **(B)** Relative fluorescence intensity values were averaged for sequential segments each 10% of the total neurite length. Fluorescence intensity varied significantly over the neurite length [1-way analysis of variance (ANOVA); $P < 0.01$]. A post-hoc analysis revealed that only the most proximal segment (soma) was significantly different than labeling in the most distal segment (growth cone) (*$P < 0.01$). Scale bar = 50 μm. $N = 8$. Color images available online at www.liebertpub.com/scd

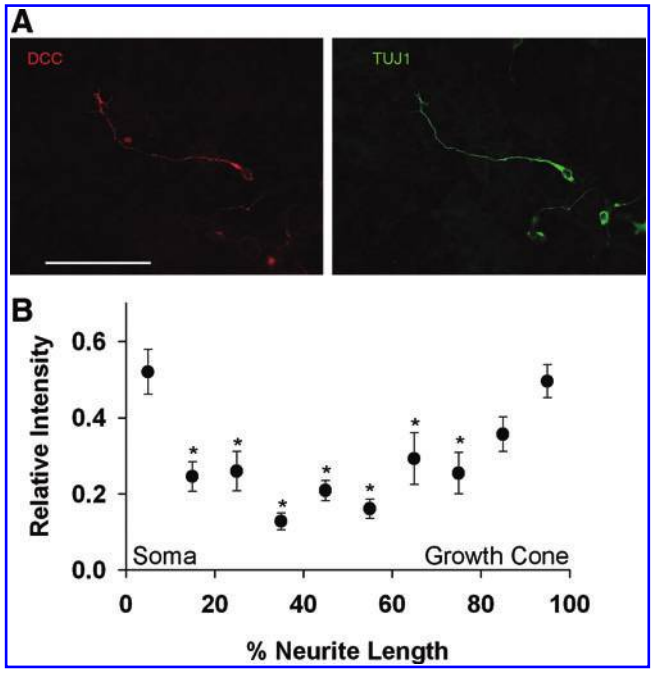

FIG. 5. DCC is preferentially localized to the cell soma and the growth cone in TUJ1-positive cells. **(A)** Induced cells were stained with anti-TUJ1 and anti-DCC as in Fig. 3. **(B)** The intensity of the fluorescence label was measured as in Fig. 4. A 1-way ANOVA was conducted showing a significant relationship between intensity and length ($P < 0.01$). A post-hoc analysis revealed that the labeling intensity was significantly greater in the soma and the growth cone than in the middle of the neurite (*$P < 0.01$). Scale bar = 50 μm. $N = 10$. Color images available online at www.liebertpub.com/scd

with the netrin$^{VI\text{-}V\text{-}Fc}$-conditioned medium and probed for netrin binding using an antibody to the human Fc tag. Anti-human immunoglobulin G (IgG) revealed extensive netrin$^{VI\text{-}V\text{-}Fc}$ binding to induced and uninduced cells treated with NCM (Fig. 6A, B), whereas cells treated with CCM exhibited faint, nonspecific label (Fig. 6C, D). When blocking antibodies to DCC and NEO1 were included with the NCM, anti-human IgG staining was diminished (Supplementary Fig. S2A, B). Western blots of whole-cell lysates were used to confirm the specificity of the anti-human IgG reactivity. Differentiated cells treated with NCM showed a single, prominent band corresponding to the expected molecular weight of netrin$^{VI\text{-}V\text{-}Fc}$ (~90 kDa, personal communication, Dr. Elke Stein, Yale University) (Fig. 6E). This reactivity was diminished when NCM was applied in the presence of blocking antibodies to DCC and NEO1 (Supplementary Fig. S2C). The 90-kDa band could be detected in NCM-alone, but was absent from CCM (Fig. 6F), suggesting that the reactive target was specifically secreted by the netrin-transfected HEKs. Therefore, the recombinant netrin$^{VI\text{-}V\text{-}Fc}$ bound *Neurog1*-induced cells, and to a lesser extent, uninduced ESCs. In contrast, induced and uninduced cells treated with CCM showed no reactivity (Fig. 6E). Results in Fig. 6 are representative of 3 to 4 biological repeats.

Aggregates of the netrin$^{VI\text{-}V\text{-}Fc}$ and untransfected HEK cells were added to *Neurog1*-induced cultures to determine any functional impact of a netrin gradient on axon outgrowth. Time-lapse images were taken in the vicinity of the HEK cells within 0.5 mm of the aggregate border. Two examples of neurites growing toward the netrin-HEK aggregate are shown in Fig. 7. This approach proved to be too challenging for high throughput quantification of axon extension or turning, since the majority of neurites initially targeted for a time-lapse series retracted due to cell death, formed connections with neighboring cells, or migrated out of the field of view. Even so, a majority of healthy neurites remaining within the imaging field were attracted to the aggregate. To examine the impact of a realistic netrin

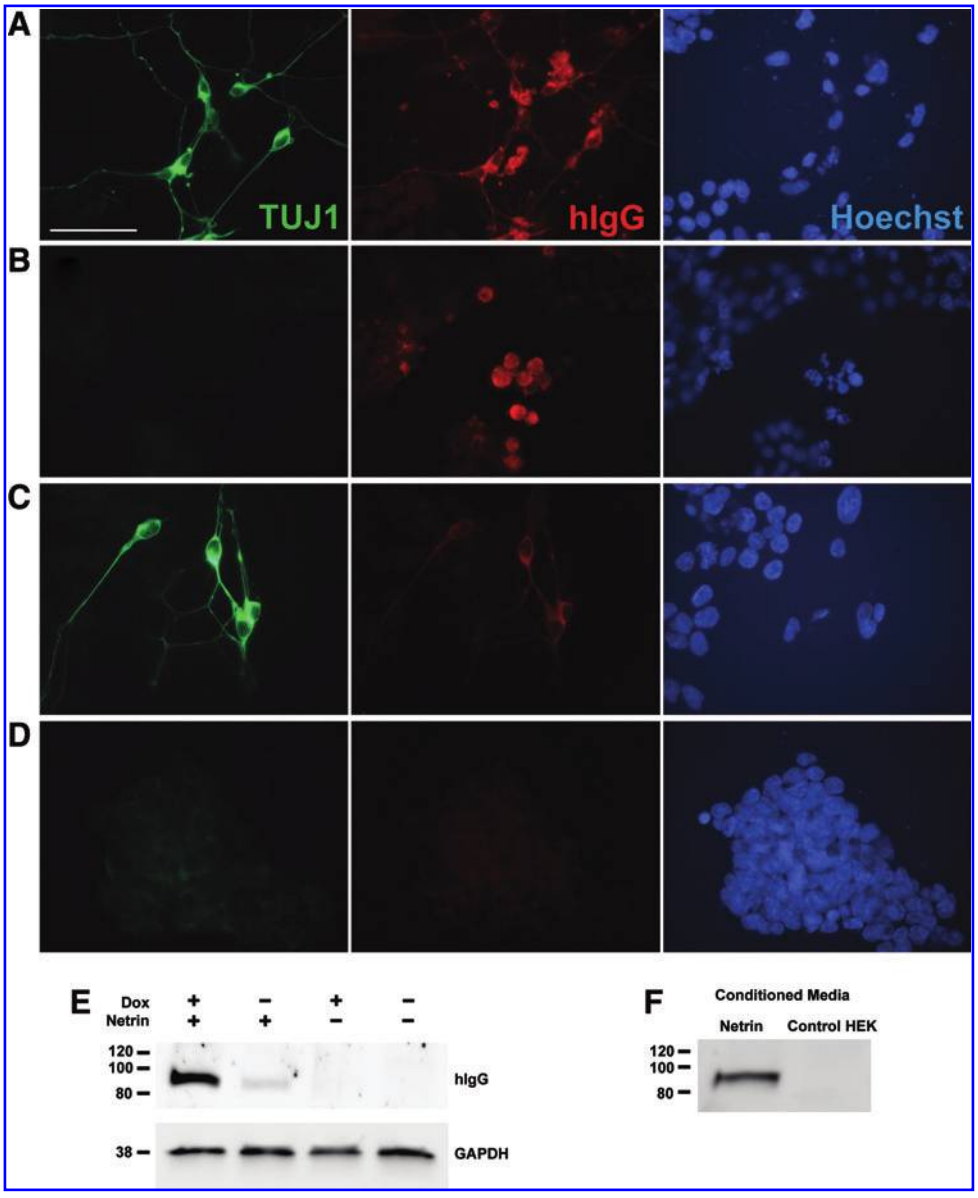

FIG. 6. Recombinant netrin binds to induced and uninduced cells. Induced and uninduced ESCs were exposed to the netrin-conditioned medium **(**NCM; **A** and **B,** respectively**),** or the control-conditioned medium (CCM) from untransfected HEK cells **(C** and **D,** respectively**)**. Preparations were stained with anti-human immunoglobulin G1 (hIgG, *red*) to visualize netrin binding and counterstained with TUJ1 (*green*) and Hoechst (*blue*). Scale bar = 50 μm. **(E)** Immunoblots from whole-cell lysates of cells treated with NCM or CCM were probed for reactivity with hIgG. A single specific band at ~90 kDa was identified, corresponding to the weight of netrin$^{VI\text{-}V\text{-}Fc}$. The blot was stripped and re-probed with anti-glyceraldehyde 3-phosphate dehydrogenase (GAPDH) as a loading control. **(F)** The same band was identified in concentrated samples of NCM, but was absent in samples of CCM from untransfected HEK cells. Color images available online at www.liebertpub.com/scd

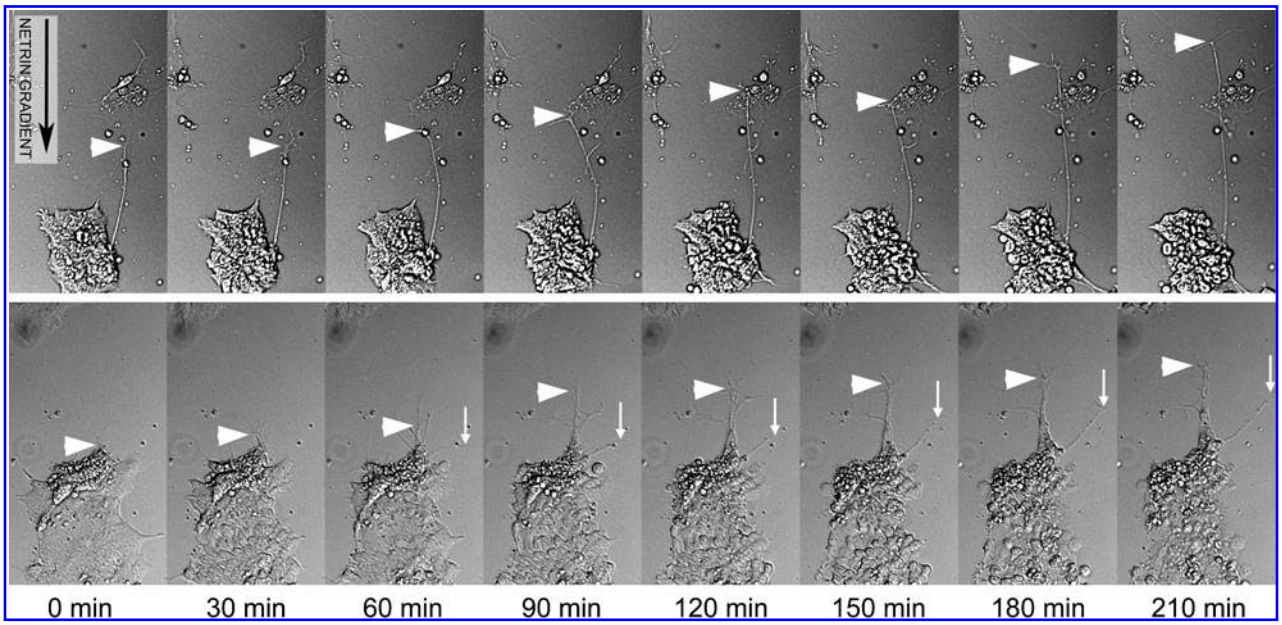

FIG. 7. Neurites are attracted toward netrin-secreting HEK cells. Aggregate HEK cells stably transfected with netrin$^{VI\text{-}V\text{-}Fc}$ were introduced to cultures after 3 days of *Neurog1* induction. Live-cell images reveal axon growth toward the netrin aggregate. A *long black arrow* points down the netrin gradient extending out from the aggregate in a radial direction. The images were oriented so that the aggregate (out of view) was positioned at the top of both image series. Growth cones are marked by *white arrowheads*. A *thin white arrow* marks another axonal projection that reoriented along the netrin gradient.

gradient, *Neurog1*-induced cells were cultured in the presence of a netrin-HEK aggregate or control-HEK aggregate for 48 h. After this time period, the preparations were fixed, stained with anti-TUJ1, and measured to determine whether growth cones aligned with the concentration gradient, turning toward or away from the aggregate. The turning angle was measured as the angle between the axon initiation segment (Fig. 8A, a) and a line drawn from the soma to the growth cone (Fig. 8A, b). Positive turning angles indicated a growth cone that had turned toward the aggregate and negative values indicated axons that turned away from the aggregate. This type of analysis provides a snapshot view in a gradient naturally created by a secreting cell source. Cells with neurites extending solely in a radial direction from the aggregate were excluded since we could not determine whether these were actively growing toward or away from the netrin source. Given the possibility of competing cues from neighboring cell types, it was important to include only those cells with a clearly identified growth cone and no apparent synaptic contact (see example in Fig. 8B). Neurons up to 4 mm from the center of the aggregate were considered for the analysis. The data were arbitrarily divided into a Near group that had a soma within 2 mm of the center of the aggregate and a Far group that were more than 2 mm away. The average turning angle for the Netrin-Near group was 15.4° ± 4.7 (Fig. 8C), a value significantly greater than that for neurons far from the netrin-secreting HEKs and for neurons both near and far from the control HEK aggregate (Tukey-Kramer post-hoc ANOVA, $P < 0.05$ for each pairwise comparison). To illustrate the netrin effect on the complete data set, the distribution of the turning angle data was plotted as cumulative percent [26] for each of the 4 experimental groups (Fig. 8D). For the Netrin-Near group, 95% of the turning angles fell between 75° and −51°. The midpoint of a curve-fit to these data, using the first derivative of a normal distribution, was 16.4°, close to the mean turning angle for this group. Distributions for the other experimental groups were similar in range, but with midpoints near 0° (95% data interval for Netrin-Far was 55° to −60°, Control-Near 50° to −53°, and Control-Far 66° to −61°). Therefore, as a distribution, the Netrin-Near data set simply shifted to more positive turning angles, suggesting that netrin uniformly affected the full population of neurons near the aggregate rather than having a disproportionately large effect on a small subset of cells.

In addition to its effect on guidance, netrin-1 reportedly increases the neurite length. This effect is nonmonotonically dependent on ligand concentration [26]. In general, length becomes larger with increasing concentration, although high concentrations have little or no effect on length. Neurite length, measured for the 10 neurons closest to the aggregate in each co-culture, averaged 302.5 ± 43.6 μm in netrin-HEK cultures and 248.1 ± 44.2 μm in control-HEK cultures. This difference was statistically insignificant (unpaired *t*-test, $P = 0.38$). It is possible that different mechanisms underlie guidance and length or that these properties are differentially affected by ligand concentration.

Discussion

Stem cell-mediated therapy has great potential for treating neurological deficits, but to do so, derived neurons must recapitulate region-specific phenotypes as well as the guidance cues that will facilitate integration with intended targets. *Neurog1*-induction in mouse ESCs recreates the transcriptional cascade, morphology, neurochemical profile [5], and electrophysiology [6] of general sensorineural phenotypes. In the current study, we found that *Neurog1*-induced neurons

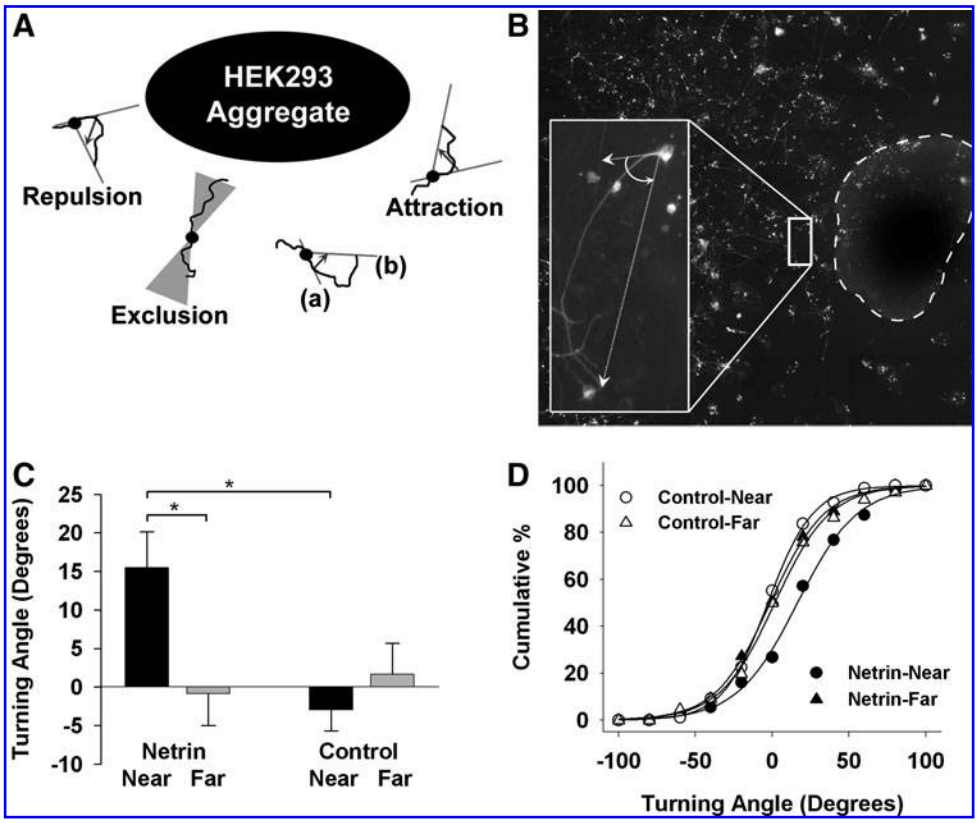

FIG. 8. Netrin-1 attracts growth cones of *Neurog1*-induced ESCs. **(A)** A schematic of the turning assay is shown. Measurements included the distance from the HEK centroid to the cell soma and the angle made by the initial axonal segment **(a)** and the growth cone **(b)**. Neurons with an initial segment pointing toward or away from the aggregate were excluded from the analysis. Positive turning angles indicate growth toward the aggregate and negative angles away. **(B)** Preparations were stained for TUJ1, imaged, and analyzed under blinded conditions for control or netrin-secreting HEKs. *Inset* shows a typical neuron contributing to the data set. **(C)** The turning angle was averaged for cells Near the aggregate (within 2 mm of centroid) and Far (>2 mm from centroid). Only cells found near the netrin-secreting aggregate were attracted by the guidance cue. (*$P < 0.05$). **(D)** The cumulative distribution of the Netrin-Near group was shifted toward positive turning angles, whereas the distributions of the other groups overlapped. $N = 55$ for Netrin-Near, 56 for Netrin-Far, 97 for Control-Near, and 67 for Control-Far.

upregulated the netrin receptors DCC and NEO1, bound netrin in a DCC/NEO1 dependent manner, and were attracted to cells secreting a recombinant form of netrin-1.

The chemoattraction response described here advances our understanding of the subtype-specific fate of *Neurog1*-induced ESCs. *Neurog1* is essential in the development of many central and peripheral neural subclasses, including vestibulocochlear, trigeminal, and a subpopulation of dorsal root ganglia [19,27,28]. While sensory neurons in these systems share many phenotypic traits, there remain some striking distinctions, including differences in firing features and ion channel expression, response to neurotrophic factors, and sensitivity to axon guidance molecules. For example, *Neurog1*-is central to the development of small diameter dorsal root ganglion neurons, which exhibit TTX-resistant sodium channels [29], responsiveness to NGF/TrkA [20], and are repelled by netrin [18]. In contrast, SGNs of the auditory nerve exhibit TTX-sensitive sodium channels [30], responsiveness to BDNF/TrkB and NT3/TrkC [31,32], and are attracted by netrin [17]. Our data add to prior molecular [5] and electrophysiological [6] evidence that *Neurog1*-induced ESCs default toward a SGN-like phenotype. It remains to be seen whether additional SGN features are recapitulated and whether other factors can be used to diversify the fate of *Neurog1*-expressing ESCs to mimic other neural subtypes.

In our cells, the attraction response was evident in short (hours) and long (2 day) cultures. Although the mean response was large and statistically reliable, turning angles varied over a wide range. Even so, the average effect and even the distribution of the turning angle data were comparable to data from other studies, including those focally applying netrin to axonal growth cones. In a Dunn chamber assay on guidance in motor neurons, the turning angle in response to netrin averaged 20° and ranged from −50° to 100° [33]. Focal application of netrin to retinal ganglion cell growth cones resulted in an average turning angle of about 20° with ~95% of the data falling between −40° and 50° [26]. In both cases, nearly 20% of the neurons exhibited negative turning angles. In our Netrin-Near data, the distribution of turning angles for each experimental group was similarly broad, spanning a range of about 120° with an average turning angle of 15° and 27% of the cells exhibiting negative turning angles. Factors contributing to the variance

in these data include the influence of other secreted and contact cues, variability in receptor density, and effects of other guidance receptors [34–36]. Nonetheless, our data are in good agreement with other studies probing the attraction of neuronal growth cones to a diffusible netrin source.

The attraction response was likely mediated by the netrin receptor DCC. The pronounced upregulation of DCC in comparison to NEO1, together with its preferential expression in the growth cone, suggests a prominent role of this receptor in the axon guidance of these cells. This conclusion is further supported by inhibition of netrin binding in the presence of blocking antibodies to this receptor. Recently, *Dcc* was identified as a putative Neurog1/NeuroD1 transcription target based on a bioinformatics analysis of promoter sequences [14]. Our data support this link and extend similar studies in native sensory systems governed by neurogenins. In addition to the effects in retinal ganglion cells discussed above, DCC-mediated chemoattraction plays a vital role in interneurons of the dorsal column [37], vagal sensory neurons in the gut [38,39], and primary auditory neurons in the cochlea [17,40]. However, the expression of *Neurog1* and DCC alone is not predictive of netrin chemoattraction. Sensory neurons of the dorsal root ganglion are dependent on neurogenins and express DCC, but are repelled by netrin-1 due to the co-expression of UNC5, a netrin receptor associated with chemorepulsion [18]. Interestingly, promoter analysis also identified UNC5c as a direct transcriptional target of Neurog1/NeuroD1, in contrast to the expression data reported here. Clearly, the relationship between fate discrimination and the downstream events that regulate axon pathfinding is complex. Further study is required to determine if Neurog1 and NeuroD1 are not only sufficient, but necessary for netrin sensitivity. Genetic induction strategies as used in our study could become a powerful tool for teasing apart the complex relationship between proneural transcription factors, pheno-subtype, and axon guidance responses. In future experiments, it will be important to both overexpress and knockdown proneural transcription factors in ESC-derived neurons to identify the degree to which bHLH genes specifically regulate certain guidance systems.

Another netrin receptor, NEO1, was extensively expressed in our cells before and after induction of *Neurog1* in both neural and non-neural cell types. Unlike DCC, NEO1 expression is broad and includes precursors in the embryonic and adult central nervous system [41]. Neogenin has a similar overall structure to DCC, but binds several ligands in addition to netrins, including repulsive guidance molecule (RGM) and cell adhesion-related/down regulated by oncogenes (CDO). Based on its breadth of expression and capacity to bind multiple ligands, it is little surprising that neogenin signaling plays a variety of roles in addition to axon guidance, including cell adhesion, migration, differentiation, and organ morphogenesis [13]. Neogenin also contributes to cell survival when interacting with RGM [42,43]. RGM/netrin-NEO1 signaling is involved in retinal ganglion cell axon guidance [44] and dorsoventral patterning in the embryonic forebrain [45]. RGM-NEO1 activity is thought to be chemorepulsive, so the impact of netrin-NEO1 on axon guidance in our cells is unclear. Further work is required to explore the functional impact of NEO1 in *Neurog1*-differentiated ESCs and in endogenous neurons that rely on the Neurog1 transcriptional cascade.

Netrins serve many functions in organogenesis, but persistent expression of this ligand into adulthood suggests additional roles in maintenance of tissue organization and regulation of regrowth [14]. Netrin expression persists in mature cochlea [16], olfactory epithelium [46], and dorsal root ganglion [47]. In some cases, continued expression in mature tissues could act favorably to guide integration of ESC-derived neurons with a netrin-secreting target. In other cases, netrin may repel regrowth or misdirect invading axons. Since netrin functions as a repulsive cue in the dorsal root ganglion, its continued expression in the adult inhibits regenerative axon growth in the damaged spinal cord [48]. A similar repulsive response may have prevented integration of dorsal root ganglion grafts introduced to the deafened ear [49,50]. These observations emphasize the need to fully characterize the guidance systems employed by ESC-derived neurons since improper receptor expression could prevent functional engraftment.

Genetic reprogramming of ESCs enables reliable, efficient generation of neurons in a particular neural lineage. Overexpression of *Neurog1* in ESCs produces neurons with several of the characteristics of SGNs, making these cells attractive candidates for regenerating the auditory nerve and other sensory ganglia requiring netrin for axon pathfinding. Before this approach can move toward clinical applications, it will be critical to identify other guidance systems at play and to fully characterize the broader impact of these chemotropic factors on the physiology of neuronal and non-neuronal cells. While the phenotypes of non-neuronal cells were unexplored in the current study, it is essential to define the functional role of netrin on all ESC-derived cell types to predict effects of the local graft environment on cell survival, migration, fate specification, and integration. Such studies will advance stem cell replacement therapy and, in the case of *Neurog1*-induced neurons, lay a foundation for relieving the devastating impact of sensory neuropathies.

Acknowledgments

This work was supported by NIH T32 DC005356, NIH T32 DC000011, and NIH P30 DC05188.

Author Disclosure Statement

There are no actual or potential conflict of interests with this report and any author.

References

1. Aboody K, A Capela, N Niazi, JH Stern and S Temple. (2011). Translating stem cell studies to the clinic for CNS repair: current state of the art and the need for a rosetta stone. Neuron 70:597–613.
2. Robertson MJ, P Gip and DV Schaffer. (2008). Neural stem cell engineering: directed differentiation of adult and embryonic stem cells into neurons. Front Biosci 13:21–50.
3. Kanda S, Y Tamada, A Yoshidome, I Hayashi and T Nishiyama. (2004). Over-expression of bHLH genes facilitate neural formation of mouse embryonic stem (ES) cells *in vitro*. Int J Dev Neurosci 22:149–156.
4. Velkey JM. (2005). Lineage differentiation of embryonic stem cells (Doctoral Dissertation). University of Michigan of Michigan, Ann Arbor, Michigan. Retrieved from Dissertations and Theses database. (UMI No. 3192805)

5. Reyes JH, KS O'Shea, NL Wys, JM Velkey, DM Prieskorn, K Wesolowski, JM Miller and RA Altschuler. (2008). Glutamatergic neuronal differentiation of mouse embryonic stem cells after transient expression of neurogenin 1 and treatment with BDNF and GDNF: *in vitro* and *in vivo* studies. J Neurosci 28:12622–12631.
6. Tong M, JL Hernandez, EK Purcell, RA Altschuler and RK Duncan. (2010). The intrinsic electrophysiological properties of neurons derived from mouse embryonic stem cells overexpressing neurogenin-1. Am J Physiol Cell Physiol 299: C1335–C1344.
7. Dent EW, F Tang and K Kalil. (2003). Axon guidance by growth cones and branches: common cytoskeletal and signaling mechanisms. Neuroscientist 9:343–353.
8. Kennedy TE and M Tessier-Lavigne. (1995). Guidance and induction of branch formation in developing axons by target-derived diffusible factors. Curr Opin Neurobiol 5: 83–90.
9. Sun KL, JP Correia and TE Kennedy. (2011). Netrins: versatile extracellular cues with diverse functions. Development 138:2153–2169.
10. Rajasekharan S and TE Kennedy. (2009). The netrin protein family. Genome Biol 10:239.
11. Moore SW, M Tessier-Lavigne and TE Kennedy. (2007). Netrins and their receptors. Adv Exp Med Biol 621:17–31.
12. De Vries M and HM Cooper. (2008). Emerging roles for neogenin and its ligands in CNS development. J Neurochem 106:1483–1492.
13. Wilson NH and B Key. (2007). Neogenin: one receptor, many functions. Int J Biochem Cell Biol 39:874–878.
14. Seo S, JW Lim, D Yellajoshyula, LW Chang and KL Kroll. (2007). Neurogenin and NeuroD direct transcriptional targets and their regulatory enhancers. EMBO J 26:5093–5108.
15. Mattar P, O Britz, C Johannes, M Nieto, L Ma, A Rebeyka, N Klenin, F Polleux, F Guillemot and C Schuurmans. (2004). A screen for downstream effectors of Neurogenin2 in the embryonic neocortex. Dev Biol 273:373–389.
16. Gillespie LN, PL Marzella, GA Clark and JA Crook. (2005). Netrin-1 as a guidance molecule in the postnatal rat cochlea. Hear Res 199:117–123.
17. Lee KH and ME Warchol. (2008). Promotion of neurite outgrowth and axon guidance in spiral ganglion cells by netrin-1. Arch Otolaryngol Head Neck Surg 134:146–151.
18. Masuda T, K Watanabe, C Sakuma, K Ikenaka, K Ono and H Yaginuma. (2008). Netrin-1 acts as a repulsive guidance cue for sensory axonal projections toward the spinal cord. J Neurosci 28:10380–10385.
19. Ma Q, Z Chen, I del Barco Barrantes, JL de la Pompa and DJ Anderson. (1998). Neurogenin1 is essential for the determination of neuronal precursors for proximal cranial sensory ganglia. Neuron 20:469–482.
20. Ma Q, C Fode, F Guillemot and DJ Anderson. (1999). Neurogenin1 and neurogenin2 control two distinct waves of neurogenesis in developing dorsal root ganglia. Genes Dev 13:1717–1728.
21. Livak KJ and TD Schmittgen. (2001). Analysis of relative gene expression data using real-time quantitative PCR and the 2(-Delta Delta C(T)) Method. Methods 25:402–408.
22. Keino-Masu K, M Masu, L Hinck, ED Leonardo, SS Chan, JG Culotti and M Tessier-Lavigne. (1996). Deleted in colorectal cancer (DCC) encodes a netrin receptor. Cell 87:175–185.
23. Roche FK, BM Marsick and PC Letourneau. (2009). Protein synthesis in distal axons is not required for growth cone responses to guidance cues. J Neurosci 29:638–652.
24. Votin V, WJ Nelson and AI Barth. (2005). Neurite outgrowth involves adenomatous polyposis coli protein and beta-catenin. J Cell Sci 118:5699–5708.
25. Kennedy TE, T Serafini, JR de la Torre and M Tessier-Lavigne. (1994). Netrins are diffusible chemotropic factors for commissural axons in the embryonic spinal cord. Cell 78:425–435.
26. de la Torre JR, VH Hopker, GL Ming, MM Poo, M Tessier-Lavigne, A Hemmati-Brivanlou and CE Holt. (1997). Turning of retinal growth cones in a netrin-1 gradient mediated by the netrin receptor DCC. Neuron 19:1211–1224.
27. Ma Q, L Sommer, P Cserjesi and DJ Anderson. (1997). Mash1 and neurogenin1 expression patterns define complementary domains of neuroepithelium in the developing CNS and are correlated with regions expressing notch ligands. J Neurosci 17:3644–3652.
28. Quinones HI, TK Savage, J Battiste and JE Johnson. (2010). Neurogenin 1 (Neurog1) expression in the ventral neural tube is mediated by a distinct enhancer and preferentially marks ventral interneuron lineages. Dev Biol 340:283–292.
29. Caffrey JM, DL Eng, JA Black, SG Waxman and JD Kocsis. (1992). Three types of sodium channels in adult rat dorsal root ganglion neurons. Brain Res 592:283–297.
30. Fryatt AG, C Vial, M Mulheran, MJ Gunthorpe and BD Grubb. (2009). Voltage-gated sodium channel expression in rat spiral ganglion neurons. Mol Cell Neurosci 42:399–407.
31. Farinas I, KR Jones, L Tessarollo, AJ Vigers, E Huang, M Kirstein, DC de Caprona, V Coppola, C Backus, LF Reichardt and B Fritzsch. (2001). Spatial shaping of cochlear innervation by temporally regulated neurotrophin expression. J Neurosci 21:6170–6180.
32. Schimmang T, J Tan, M Muller, U Zimmermann, K Rohbock, I Kopschall, A Limberger, L Minichiello and M Knipper. (2003). Lack of Bdnf and TrkB signalling in the postnatal cochlea leads to a spatial reshaping of innervation along the tonotopic axis and hearing loss. Development 130: 4741–4750.
33. Bai G, O Chivatakarn, D Bonanomi, K Lettieri, L Franco, C Xia, E Stein, L Ma, JW Lewcock and SL Pfaff. (2011). Presenilin-dependent receptor processing is required for axon guidance. Cell 144:106–118.
34. Hu G and ER Fearon. (1999). Siah-1 N-terminal RING domain is required for proteolysis function, and C-terminal sequences regulate oligomerization and binding to target proteins. Mol Cell Biol 19:724–732.
35. Galko MJ and M Tessier-Lavigne. (2000). Function of an axonal chemoattractant modulated by metalloprotease activity. Science 289:1365–1367.
36. Stein E and M Tessier-Lavigne. (2001). Hierarchical organization of guidance receptors: silencing of netrin attraction by slit through a Robo/DCC receptor complex. Science 291: 1928–1938.
37. Kubota C, T Nagano, H Baba and M Sato. (2004). Netrin-1 is crucial for the establishment of the dorsal column-medial lemniscal system. J Neurochem 89:1547–1554.
38. Ratcliffe EM, SU Setru, JJ Chen, ZS Li, F D'Autreaux and MD Gershon. (2006). Netrin/DCC-mediated attraction of vagal sensory axons to the fetal mouse gut. J Comp Neurol 498: 567–580.
39. Ratcliffe EM, F D'Autreaux and MD Gershon. (2008). Laminin terminates the Netrin/DCC mediated attraction of vagal sensory axons. Dev Neurobiol 68:960–971.
40. Anderson M, M Bostrom, K Pfaller, R Glueckert, A Schrott-Fischer, B Gerdin and H Rask-Andersen. (2006). Structure

and locomotion of adult *in vitro* regenerated spiral ganglion growth cones—a study using video microscopy and SEM. Hear Res 215:97–107.
41. Fitzgerald DP, D Bradford and HM Cooper. (2007). Neogenin is expressed on neurogenic and gliogenic progenitors in the embryonic and adult central nervous system. Gene Expr Patterns 7:784–792.
42. Shoemaker LD, NM Orozco, DH Geschwind, JP Whitelegge, KF Faull and HI Kornblum. (2010). Identification of differentially expressed proteins in murine embryonic and postnatal cortical neural progenitors. PLoS One 5:e9121.
43. Matsunaga E, S Tauszig-Delamasure, PP Monnier, BK Mueller, SM Strittmatter, P Mehlen and A Chedotal. (2004). RGM and its receptor neogenin regulate neuronal survival. Nat Cell Biol 6:749–755.
44. Matsunaga E, H Nakamura and A Chedotal. (2006). Repulsive guidance molecule plays multiple roles in neuronal differentiation and axon guidance. J Neurosci 26:6082–6088.
45. Wilson NH and B Key. (2006). Neogenin interacts with RGMa and netrin-1 to guide axons within the embryonic vertebrate forebrain. Dev Biol 296:485–498.
46. Astic L, V Pellier-Monnin, D Saucier, C Charrier and P Mehlen. (2002). Expression of netrin-1 and netrin-1 receptor, DCC, in the rat olfactory nerve pathway during development and axonal regeneration. Neuroscience 109: 643–656.
47. Wehrle R, E Camand, A Chedotal, C Sotelo and I Dusart. (2005). Expression of netrin-1, slit-1 and slit-3 but not of slit-2 after cerebellar and spinal cord lesions. Eur J Neurosci 22:2134–2144.
48. Park JI, IA Seo, HK Lee, HT Park, SW Shin, YM Park and KJ Ahn. (2007). Netrin inhibits regenerative axon growth of adult dorsal root ganglion neurons *in vitro*. J Korean Med Sci 22:641–645.
49. Hu Z, M Ulfendahl and NP Olivius. (2004). Survival of neuronal tissue following xenograft implantation into the adult rat inner ear. Exp Neurol 185:7–14.
50. Hu Z, M Ulfendahl, DM Prieskorn, P Olivius and JM Miller. (2009). Functional evaluation of a cell replacement therapy in the inner ear. Otol Neurotol 30:551–558.

Address correspondence to:
Dr. Robert Keith Duncan
Department of Otolaryngology
Kresge Hearing Research Institute
University of Michigan
1150 West Medical Center Drive
5323A Medical Science Building I
Ann Arbor, MI 48109-5616

E-mail: rkduncan@umich.edu

Received for publication August 5, 2011
Accepted after revision April 17, 2012
Prepublished on Liebert Instant Online April 18, 2012

This article has been cited by:

1. Erin K. Purcell, Amy Yang, Liqian Liu, J. Matthew Velkey, Marti M. Morales, R. Keith Duncan. 2013. BDNF profoundly and specifically increases KCNQ4 expression in neurons derived from embryonic stem cells. *Stem Cell Research* **10**:1, 29-35. [CrossRef]